Hindawi
Journal of Chemistry
Volume 2018, Article ID 5137694, 8 pages
https://doi.org/10.1155/2018/5137694

Research Article

Enhanced As (V) Removal from Aqueous Solution by Biochar Prepared from Iron-Impregnated Corn Straw

Jiaming Fan,[1] Xin Xu,[1] Qunli Ni,[1] Qi Lin ,[1,2] Jing Fang,[1] Qian Chen,[1] Xiaodong Shen,[3] and Liping Lou[1,2]

[1]*Department of Environmental Engineering, Zhejiang University, Hangzhou 310058, China*
[2]*Key Laboratory of Water Pollution Control and Environmental Safety of Zhejiang Province, Hangzhou, China*
[3]*Institute of Hangzhou Environmental Science, Hangzhou 310014, China*

Correspondence should be addressed to Qi Lin; linqi@zju.edu.cn

Received 5 January 2018; Accepted 13 February 2018; Published 3 April 2018

Academic Editor: Xiao-San Luo

Fe-loaded adsorbents have received increasing attention for the removal of arsenic in contaminated water or soil. In this study, Fe-loaded biochar was prepared from iron-impregnated corn straw under a pyrolysis temperature of 600°C. The ratio of crystalline Fe oxides including magnetite and natrojarosite to amorphous iron oxyhydroxide in the composite was approximately 2 : 3. Consisting of 24.17% Fe and 27.76% O, the composite exhibited a high adsorption capacity of 14.77 mg g^{-1} despite low surface areas (4.81 m^2 g^{-1}). The pH range of 2.0–8.0 was optimal for arsenate removal and the adsorption process followed the Langmuir isotherms closely. In addition, pseudo-second-order kinetics best fit the As removal data. Fe oxide constituted a major As-adsorbing sink. Based on the X-ray diffraction spectra, saturation indices, and selective chemical extraction, the data suggested three main mechanisms for arsenate removal: sorption of arsenate, strong inner-sphere surface complexes with amorphous iron oxyhydroxide, and partial occlusion of arsenate into the crystalline Fe oxides or carbonized phase. The results indicated that the application of biochar prepared from iron-impregnated corn straw can be an efficient method for the remediation of arsenic contaminated water or soil.

1. Introduction

With the rapid development of urban space and intensification of agricultural and industrial activities, chemical pollution has become a serious environmental issue, particularly in China [1, 2]. Arsenic, as a potential carcinogen, is associated with a variety of human diseases, such as cardiovascular diseases, liver fibrosis, kidney disorders, blood toxicity, and chronic lung disease [3]. Arsenic's potential to pose a hazard to human health has prompted the establishment of more stringent environmental regulations and hence the development of innovative and cost-effective technologies for the treatment of arsenic in the environment. [4–7]. Recently, the thermochemical conversion of agricultural waste has received increasing attention in the last decades due to its potential application in pollutant removal [8]. Samsuri et al. [9] reported that the maximum adsorption capacity for biochars prepared from empty fruit bunch and rice husk is 5.5 and 7.1 mg/g for As (V), respectively. Agrafioti et al. [10] reported that the removal efficiency of As (V) was about 25% in rice husk-derived biochars, lower than 65% in soils. Similar results were also observed in biochars prepared from pine needle and straws [11]. A search for improved and inexpensive materials is still underway [12]. Yao et al. [13] reported that Fe-loaded activated carbon had the removal rate of more than 95% for As (V). Using iron-impregnated sawdust, Liu et al. [4] successfully synthesized Fe_3O_4-loaded biochar for both arsenate removal and magnetic separation. Fe-loaded biochars from empty fruit bunch and rice husk achieved the maximum adsorption capacity of 45.2 and 16.0 mg/g for As (V), almost 2~8 times of that in the companion biochar without iron loaded [9]. The results indicated that the effectiveness of arsenic removal was closely related to the amount of iron loaded, characteristics of the media supporting the iron oxide, and synthetic conditions [4, 14]. The characteristics of biochars derived from agricultural residues vary greatly depending on the type of feedstock used, pyrolysis temperature, pyrolysis atmosphere, and activation

treatment [15]. We leveraged this variability to find and optimize a suitable and cheap material with the desired properties for supporting iron oxide.

In this study, biochar derived from iron-impregnated corn straw was prepared and utilized as a potential green adsorbent for arsenate removal. The produced composite was characterized by Fourier transform infrared (FTIR), X-ray diffraction (XRD), BET-N_2 surface area, and elemental analyses combined with chemical extractions. We report equilibrium and kinetic experiments of As(V) absorption and illustrate the mechanisms of As(V) removal through the interpretation of the adsorption data, determination of arsenic speciation using the sequential chemical extraction method, and calculation of the saturation indices for the different arsenic precipitation phases.

2. Materials and Methods

2.1. Materials. The maize straws used in this study were obtained from Tongxiang in Zhejiang province. As(V) standard stock solution (1000 mg L^{-1}) was prepared from $Na_2HAsO_4{\cdot}7H_2O$ and preserved in a brown reagent bottle.

2.2. Preparation of Biochars. The corn straws were dried at 80°C in an oven and ground to pass through 20-mesh sieve. It was mixed with 1.0 mol L^{-1} $FeCl_3$ and 50% H_2SO_4 according to a straw to $FeCl_3$ to H_2SO_4 ratio of 1 : 10 : 5 (g : mL : mL) and then ultrasonicated for 2 h and aged at 60°C for 12 h [4]. After suction separation, the recovered residue was dried at 80°C in an oven for 24 h, packed into a capped-ceramic container, and sealed to exclude as much air as possible. The carbonization was conducted in a temperature-controlled muffle furnace at 600°C for 2 h. Thereafter the furnace was turned off and the retort chamber was allowed to cool to room temperature. The iron-loaded biochar (CS-Fe) was ground to a fine powder and passed through a 0.2 mm sieve. As a control, companion biochar without iron loaded was also prepared and designated as CS.

2.3. Characterization of the Biochars. The total C, H, and N contents in the biochar samples were analyzed with an element analyzer (EA 1112, Italy). The yields of the biochars were measured by the ratio of the biochar's weight before and after pyrolysis. Ash content was determined after heating at 550°C for 3 h in a muffle furnace. The inorganic element composition of the biochars was examined after digestion with a mixture of HNO_3-HCl-$HClO_4$ acids. It was then analyzed for the total K, Ca, Fe, Mn, Cu, Zn, Pb, P, and As contents by inductively coupled plasma-atomic emission spectrometry (ICP-AES) (iCAP6300DUO, Thermo, America). The pH of the biochar was determined using the composite electrode method at the ratio of 1 : 10 water [16]. The point of zero charge (pH_{pzc}) was determined using methods outlined in the literature [17].

The FTIR spectra were carried out by mixing biochar with KBr in a ratio of 1 : 150 and scanning in the wavenumber range of 400–4000 cm^{-1} at a resolution of 4 cm^{-1} (IR PRESTIGE-21, Shimadzu, Japan) [18]. The surface oxygenic functional groups were determined according to the Boehm titration method [19]. XRD patterns of the biochars were determined on a power X-ray diffraction system using Cu Kα (λ = 1.54 Å) radiation at 40 kV and 40 mA (X-pert Powder, PANalytical B.V., Netherlands). The samples were scanned from 10° to 80° with a scan speed of 2° per minute. Surface area and pore size were measured using a BET-N_2 SA analyzer (Tristar ll3020, MIC, America).

2.4. Adsorption Studies. The batch adsorption experiments were performed by mixing 20 mL of a 0.01 M $NaNO_3$ solution containing 0–150 mg L^{-1} As(V) with the desired weight of biochar samples in 100-mL conical flasks. The flasks were then shaken at 200 rpm in a constant temperature mechanical shaker (30°C) for a preset time. The solutions were centrifuged at 3000 rpm for 10 min and filtrated through 0.45 μm filters. The concentrations of As were analyzed by ICP-AES. The effects of the biochars dose (0–10 g L^{-1}), initial solution pH (2.0–12.0), and contact time (0–24 h) were studied. Triplicates were performed for each sorption experiment.

The isotherm data were analyzed by Langmuir and Freundlich equations expressed as follows:

$$\text{Langmuir: } \frac{1}{q_e} = \frac{1}{kq_mC_e} + \frac{1}{q_m},$$
$$\text{Freundlich: } q_e = k_f \cdot {C_e}^{1/n}, \tag{1}$$

where q_e (mg g^{-1}) is the amount of solute adsorbed per unit weight at equilibrium; C_e (mg L^{-1}) is the equilibrium concentration of As (V) in solution; q_m (mg/g) and k (L mg^{-1}) are the maximum capacities of adsorption for a monolayer coverage and the affinity coefficient, respectively [20]; k_f (mg/g·(L/mg)$^{1/n}$) and $1/n$ are the Freundlich capacity coefficient and intensity constant, respectively.

In order to evaluate the kinetic process, the Lagergren-first-order and pseudo-second-order fits of the experimental data were compared

$$\text{Lagergren-first-order: } \log\left(q_e - q_t\right) = \log\left(q_e\right) - \frac{k_1 t}{2.303},$$
$$\text{pseudo-second-order: } \frac{t}{q_t} = \frac{1}{k_2 {q_e}^2} + \frac{t}{q_e}, \tag{2}$$

where q_t and q_e (mg g^{-1}) are the amounts of arsenic adsorbed at time t and equilibrium time, respectively; k_1 and k_2 are the pseudo-first-order rate constant (1/h) and pseudo-second-order rate constant (g mg^{-1} h^{-1}), respectively.

2.5. Arsenic Speciation in the Adsorbent. Samples for speciation analysis were prepared by reacting 1 g of CS-Fe with 200 mL of a 0.01 M $NaNO_3$ solution containing 40 mg L^{-1} As(V). The concentrations of K, Na, Ca, Mg, Fe, Mn, P, and S in the solution were determined by ICP-AES. Nitrate-nitrogen (NO_3-N) and chloride (Cl^-) were determined by ultraviolet spectrophotometry and a silver nitrate titration,

Table 1: Characteristics of the biochars.

	Unit	CS	CS-Fe
Element analysis			
C	%	64.14	38.08
H	%	1.92	1.44
O	%	11.44	27.76
N	%	2.09	1.01
H/C[(a)]		0.36	0.45
O/C		0.13	0.55
Ash	%	20.41	31.72
Mineral			
K	%	5.88	3.42
Ca	%	0.72	0.22
Fe	%	0.08	24.17
Mn	%	0.01	0.01
P	%	0.36	0.04
Trace metals			
Cu	$mgkg^{-1}$	21.20	49.58
Zn	$mgkg^{-1}$	96.18	27.01
Pb	$mgkg^{-1}$	9.18	14.3
As	$mgkg^{-1}$	-[(b)]	-
Functional group			
Acid sites	$mequivg^{-1}$	0.28	2.08
Basic sites	$mequivg^{-1}$	1.33	0.027
BET analysis			
Specific surface area	m^2g^{-1}	0.74	4.81
Pore volume	cm^3g^{-1}	0.0011	0.012
Others			
pH		10.89	2.55
pH_{pzc}		2.75	6.93
Yield	%	33.24	25.01

Notes. [(a)]H/C: atomic ratio of hydrogen to carbon; [(b)]-: not detectable.

respectively. The results including pH and anion and cation concentrations were used in the speciation model Visual MINTEQ for calculating the saturation indices (SI) for the different precipitation phases.

A sequential chemical extraction method was used for the determination of arsenic speciation in the adsorbent as proposed by Cances et al. [21]. The four arsenic forms including the sulfate exchangeable, specially adsorbed, bound to amorphous iron oxyhydroxide and residual fractions were studied (Table S1).

3. Results and Discussion

3.1. Characterization of Biochars. Selected properties of the CS and CS-Fe are listed in Table 1. The content of O in the CS-Fe (27.76%) was higher than that in the CS (11.44%), suggesting that the CS-Fe had a large proportion of oxygen-containing functional groups. It was also confirmed by the Boehm titration that the total functional groups in the CS-Fe were higher than that in the CS (Table 1). The lower carbon content and much higher ash content for CS-Fe when compared with the CS were consistent with the introduction of iron oxide in the former. The higher H/C ratio of the CS-Fe over CS indicated that more original organic matter was preserved in the iron-loaded biochar and showed lower overall aromaticity. The higher O/C ratios of the CS-Fe indicated higher polarity when compared to CS [22].

The total P, K, and Ca proportions in CS were 0.36%, 5.88%, and 0.72%, respectively, much higher than those in CS-Fe (0.04%, 3.42%, and 0.22%, resp.). This was likely due to the chemical treatment by H_2SO_4 which caused the leaching of P, K, and Ca in the CS-Fe. The content of Fe in the CS-Fe was 24.17%, 302 times that of Fe in the CS, indicating that CS-Fe was successfully loaded with iron. The BET surface area and pore volume of the CS were $0.74\,m^2\,g^{-1}$ and $0.0011\,cm^3\,g^{-1}$, respectively. Fe-impregnated biochar showed increase of both surface area ($4.81\,m^2\,g^{-1}$) and pore volume ($0.012\,cm^3\,g^{-1}$), suggesting that activation by sulfuric acid pretreatment was probably beneficial for the development of pore structure, which also increased the specific surface area. A much higher pH_{pzc} value of 6.93 for the CS-Fe versus 2.75 in the CS was observed; therefore, it was expected that the

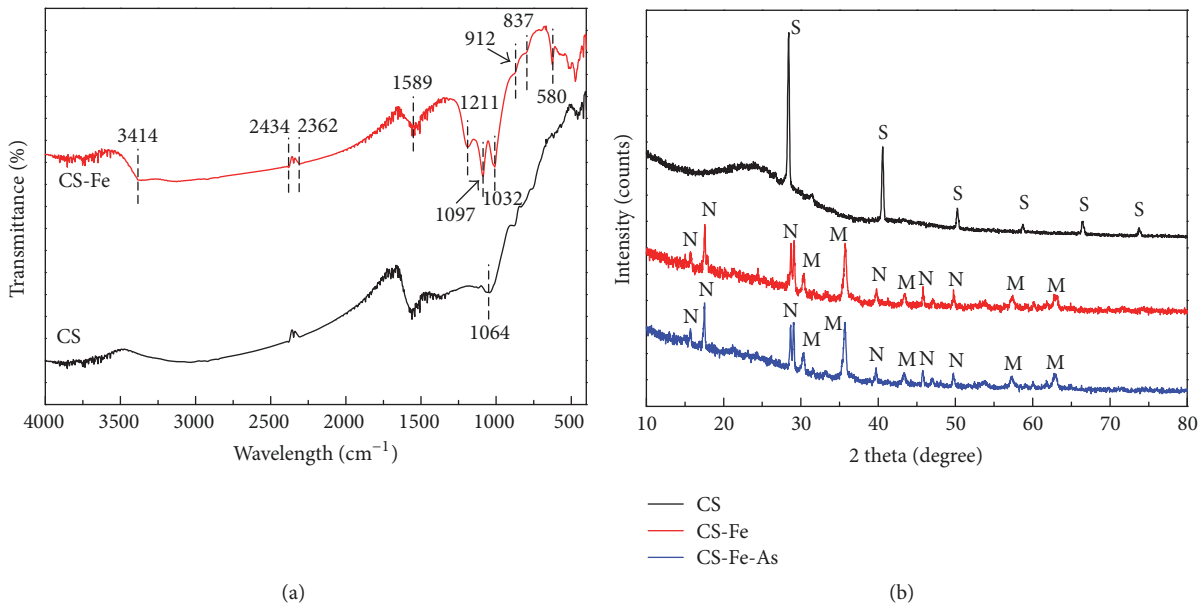

FIGURE 1: The FTIR spectra (a) and the XRD spectra (b) of CS and CS-Fe. The typical peaks of XRD spectra were labeled as follows: S, sylvite; M, magnetite; N, natrojarosite.

CS-Fe would be more conducive to the adsorption of anionic arsenate.

FTIR spectra were obtained for both the CS and CS-Fe samples (Figure 1(a)). The stretching vibration for C≡C corresponds to the peaks at 2362 and 2434 cm^{-1} [18]. The peak at 1589 cm^{-1} is the aromatic ring "breathing" vibrations [18] and the peaks at 837 and 912 cm^{-1} are assigned to the 1,3,5-trisubstituted aromatic ring (δCH out-off-plane) [23]. The new peak that appears at approximately 580 cm^{-1} in the CS-Fe spectrum is characteristic of the Fe-O stretching vibration [24]. The broader absorption band at 3414 cm^{-1} and sharp peaks at 1211 and 1097 cm^{-1} are assigned to the stretching of -OH, epoxy C-O, and C-O-C, respectively, which differed greatly in the CS and CS-Fe. This was likely due to the preservation of the original structure in the pyrolysis process in the presence of iron oxide.

The XRD patterns of CS and CS-Fe are compared in Figure 1(b). The presence of sylvine in the CS pattern was confirmed by peaks at 28.4°, 40.5°, 50.2°, 58.7°, 66.5°, and 73.7° (2θ). The peaks at 28.4°, 40.5°, 66.5°, and 73.7° disappeared in the CS-Fe pattern due to the pretreatment with sulfuric acid. The strong peaks of magnetite (Fe_3O_4) at 30.4°, 35.7°, 43.6°, 57.3°, and 62.9° (2θ) and natrojarosite ($NaFe_3(SO_4)_2(OH)_6$) at 15.8°, 17.5°, 29.1°, 40.2°, 45.8°, and 49.7° (2θ) were clearly observed in the CS-Fe patterns in both the presence and absence of As loading, suggesting that iron oxides with good crystalline structure were formed and loaded on the biochar.

3.2. Adsorption of As(V)

3.2.1. Adsorbent Dosage and Solution pH. The influence of additive dosage of CS-Fe (0 to 10 g L^{-1}) on As adsorption was studied (Figure S1). The removal efficiency of As (V) by CS-Fe increased rapidly from 2.2% to 96% as the adsorbent dose was increased from 0.4 to 5 g L^{-1}. Further increase in the adsorbent dosage had no significant effect on the removal of As (V). Therefore, the dosage of 5 g L^{-1} was selected as the optimum adsorbent dosage for the adsorption experiments.

The solution pH plays a key role in the removal of arsenic, as it influences the surface charge of the adsorbent and the forms of arsenic in solution [25]. Effects of pH on As (V) adsorption by CS and CS-Fe were investigated in the pH range from 2.0 to 12.0, with the initial As (V) concentration of 40 mg L^{-1}. It can be seen in Figure 2 that the removal efficiency of As (V) by CS and CS-Fe varied greatly in the pH range studied which clearly indicated the influence of solution pH on the adsorption process. In the case of CS, pH 4 was more suitable for As (V) removal from solution, while CS-Fe was effective with a larger pH range of 2.0–8.0. These results are similar to that of Zhu et al. [14] for As(V) adsorption on Fe_3O_4-loaded honeycomb briquette cinders, but slightly different from that of Liu et al. [4] who reported that the maximum As(V) removal efficiency was achieved at pH 8.0 by Fe_3O_4-loaded sawdust biochar. The main factors influencing the adsorption process are As (V) species and the surface charge of the adsorbents. Due to the increase in the pH_{pzc} value, the surface of CS-Fe was positively charged at pH < pH_{pzc} 6.93 for the CS-Fe and conducive to the adsorption of $H_2AsO_4^-$ (Figure S2). In an alkaline medium, however, the surface of CS-Fe is negatively charged and most As (V) species exist as $HAsO_4^{2-}$ and AsO_4^{3-} (Figure S2). The adsorption of As (V) thus decreased as a result of enhanced electrostatic repulsion [4]. Similarly, the higher As (V) removal efficiency that occurred at pH 4 for the control biochar (CS) can also be illustrated by the As (V) species and pH_{pzc}. As showed in Table 1, the surface of CS was negatively charged at pH > pH_{pzc} 2.75 and not conducive to the adsorption of $H_2AsO_4^-$ (Figure S2) at the higher pH,

Table 2: Regression parameters of isotherms of As (V).

Sample	Langmuir			Freundlich		
	q_m (mg g^{-1})	k (L mg^{-1})	R^2	k_f ((L mg^{-1})$^{1/n}$ · mg g^{-1})	$1/n$	R^2
CS-Fe	14.77	2.97	0.9968	7.95	0.31	0.8358
CS	2.86	0.01	0.9492	6.16	1.18	0.9041

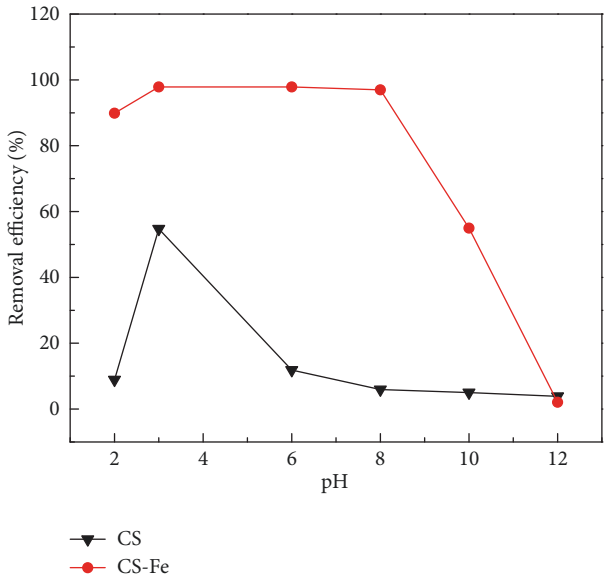

Figure 2: Effect of solution pH on the adsorption of As(V) for CS and CS-Fe (adsorbent dose 5 g L^{-1}; temperature 30°C; As(V) concentration 40 mg L^{-1}).

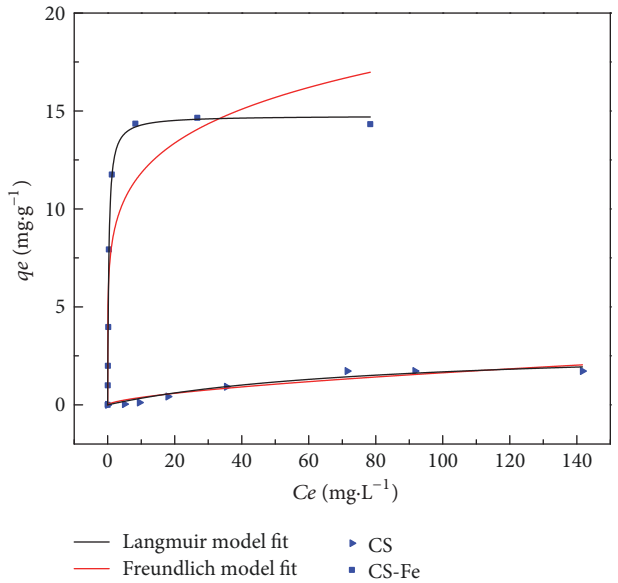

Figure 3: Adsorption isotherms of As(V) on CS-Fe and CS (adsorbent dose 5 g L^{-1}; pH 3.0; temperature 30°C).

while at pH 2, the surface was positively charged but As (V) species exist as H_3AsO_4.

3.2.2. Adsorption Isotherms. Adsorption isotherms of As by CS-Fe and CS were compared (Figure 3). Adsorption potentials of CS-Fe were much higher than that of CS, indicating a positive role of iron oxides for enhanced adsorption of As (V). The regression parameters of isotherms are listed in Table 2. It is clear that both the CS-Fe and CS followed the Langmuir-type isotherm with correlation coefficients R^2 in the range from 0.9492 to 0.9968. The Langmuir model assumes that the adsorption of the molecule occurs on a homogeneous surface as a monolayer, while the Freundlich model is an empirical equation based on a heterogeneous surface [4]. The data fit best to the Langmuir-type, implying that the adsorption of As occurs on a homogeneous surface by monolayer adsorption [14]. Conversely, using Fe_3O_4-loaded biochar prepared from sawdust, Liu et al. [4] reported that the adsorption process followed the Freundlich isotherm model at pH 8.

CS-Fe exhibited excellent immobilization capacities for As (V). The maximum adsorption capacity estimated by the Langmuir model was 14.77 mg g^{-1}, almost fivefold larger than that of CS (2.86 mg g^{-1}). The affinity coefficient of adsorption, k, varied greatly with a value of 2.97 L mg^{-1} for the CS-Fe, about 300 times that of the CS. A comparison between CS-Fe and other Fe-loaded adsorbents showed that the maximum adsorption capacity of As(V) by CS-Fe was moderately greater than iron-containing granular activated carbon (6.57–10.5 mg g^{-1}) [12], iron-containing mesoporous carbon (5.2 mg g^{-1}), and Fe_3O_4-loaded honeycomb briquette cinders (2.42 mg g^{-1}) [14], but much lower than Fe_3O_4-loaded sawdust biochar, which had the adsorption capacity of 204.2 mg g^{-1} [4]. Factors such as iron oxide species, amount of iron loaded, and dispersion and surface accessibility of iron within the carbon likely affected the As(V) removal [26]. Due to the high content of oxygen in CS-Fe (27.76%), the biochar swells in water and permits sorption inside the solid as well as on its pore surfaces, leading to high sorption capacities at low surface areas [18].

3.2.3. Kinetic Study. The adsorption of As (V) onto CS-Fe was quite rapid. At the initial concentration of 25 and 40 mg L^{-1}, 94–97% of As was removed within the first 15 min (Figure 4).

Table 3 shows the Lagergren-first-order and pseudo-second-order rate constants for As (V) on CS-Fe. With correlation coefficient $R^2 > 0.999$, the adsorption kinetics for As (V) onto CS-Fe are best described by pseudo-second-order model. The higher the initial As concentration, the lower the pseudo-second-order rate constant. Since the pseudo-second-order model usually assumes that chemisorption of an adsorbate on an adsorbent is the rate-limiting step [27], it

Table 3: Parameters of kinetic models for As(V) onto CS-Fe.

Kinetic models	Parameters	25 mg L^{-1}	40 mg L^{-1}
Lagergren-first-order	q_e (mg g^{-1})	5.67	7.87
	k_1 (h^{-1})	3.29	3.34
	R^2	0.9993	0.9953
Pseudo-second-order	q_e (mg g^{-1})	5.68	7.93
	k_2 (g mg^{-1} h^{-1})	9.12	5.13
	R^2	0.9999	0.9999

Table 4: Calculation of saturation indices (SI) for precipitation phases using the equilibrium concentrations in solution at the initial As (V) of 40 mg L^{-1} in the CS-Fe.

Phase	Reaction	log Ksp	SI[(a)]
$FeAsO_4{\cdot}2H_2O$	$FeAsO_4{\cdot}2H_2O = Fe^{3+} + AsO_4^{3-} + 2H_2O$	−20.2	−3.525
$AlAsO_4{\cdot}2H_2O$	$AlAsO_4{\cdot}2H_2O = Al^{3+} + AsO_4^{3-} + 2H_2O$	−15.8	−9.275
$Ca_3(AsO_4)_2{\cdot}4H_2O$	$Ca_3(AsO_4)_2{\cdot}4H_2O = 3Ca^{2+} + 2AsO_4^{3-} + 4H_2O$	−18.9	−33.105
$Ca_5(AsO_4)_3OH$	$Ca_5(AsO_4)_3OH = 5Ca^{2+} + 3AsO_4^{3-} + OH^-$	−40.12	−51.179
$Ca_4(OH)(AsO_4)_2{\cdot}4H_2O$	$Ca_4(OH)(AsO_4)_2{\cdot}4H_2O = 4Ca^{2+} + 2AsO_4^{3-} + OH^- + 4H_2O$	−27.49	−51.098

Notes. [(a)]Calculations performed using the Visual MINTEQ speciation model.

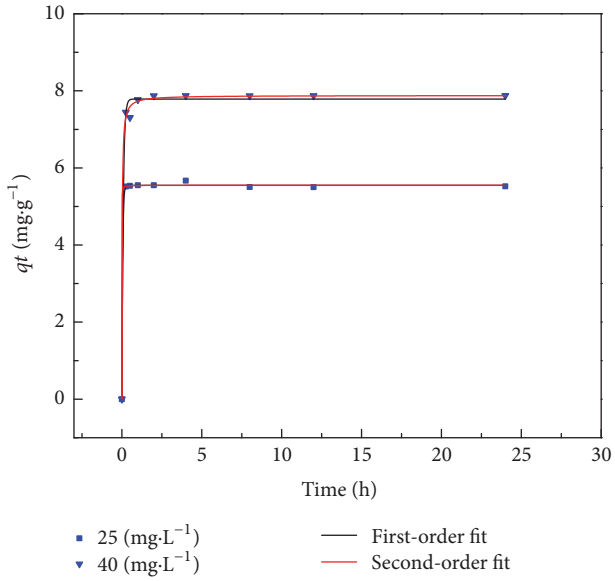

Figure 4: Adsorption kinetics of As(V) by CS-Fe (adsorbent dose 5 g L^{-1}; temperature 30°C).

is inferred that As (V) was likely adsorbed on the surface of CS-Fe via chemical interaction.

3.3. Possible Mechanism for Arsenate Removal

3.3.1. As Precipitation. Table 4 presents the saturation indices (SI) of As precipitates using equilibrium concentrations in solution at the initial As (V) concentration of 40 mg L^{-1} in the CS-Fe. The solution is undersaturated with $FeAsO_4{\cdot}2H_2O$, $AlAsO_4{\cdot}2H_2O$, $Ca_3(AsO_4)_2{\cdot}4H_2O$, $Ca_5(AsO_4)_3{\cdot}OH$, and $Ca_4(OH)(AsO_4)_2{\cdot}4H_2O$, which suggests that the formation of precipitates in the CS-Fe is thermodynamically unfavorable. Using vibrational spectroscopy, Goldberg and Johnston [28] observed that the IR and Raman spectra of As (V) adsorbed to Fe oxide samples are distinct from that of Fe arsenate salts, indicating that As (V) is bound as a surface complex and not as a precipitated solid phase. In this study, the XRD spectra for CS-Fe before and after As addition are shown in Figure 1(b). No new crystalline peak emerged in the As-loaded CS-Fe, suggesting the absence of crystalline arsenic precipitates.

3.3.2. Surface Adsorption Mechanism. Selective chemical extractions were performed on the As-loaded CS-Fe. The sulfate solution is involved in the extraction of exchangeable arsenic, the phosphate solution is typically used to remove specifically adsorbed arsenic, and the oxalate solutions involved in the extraction of arsenic associated with amorphous iron oxides. As shown in Figure 5, most of the Fe was released in the oxalate solution, accounting for about 60% of the Fe in the CS-Fe, which suggested that amorphous iron oxyhydroxide was the dominant species in the iron oxide-loaded biochar. Crystalline Fe oxides including magnetite and natrojarosite likely composed less than 40% of the CS-Fe biochar. The majority of As in the CS-Fe was also associated with amorphous iron oxyhydroxide, accounting for 52.26% of the total, suggesting the strong inner-sphere complexes that arsenate forms with iron oxide surfaces were a major mechanism for As adsorption by CS-Fe. The specifically adsorbed form was 28.23% of total arsenic, indicating that the specific anion exchange mechanism was also important in this system, and the presence of other anions such as PO_4^{3-} may inhibit the removal of As. In a study on the effect of interfering ion on the As (V) removal, Zhu et al. [14] observed that PO_4^{3-} with a concentration range of 0.1–10 mM resulted in a reduction of arsenic removal efficiency by 66.8–86.2%. Residual As comprised 18.38% of total arsenate, which likely represents the arsenate incorporated into the structures of crystalline Fe oxides [29] or the carbonized phase. These

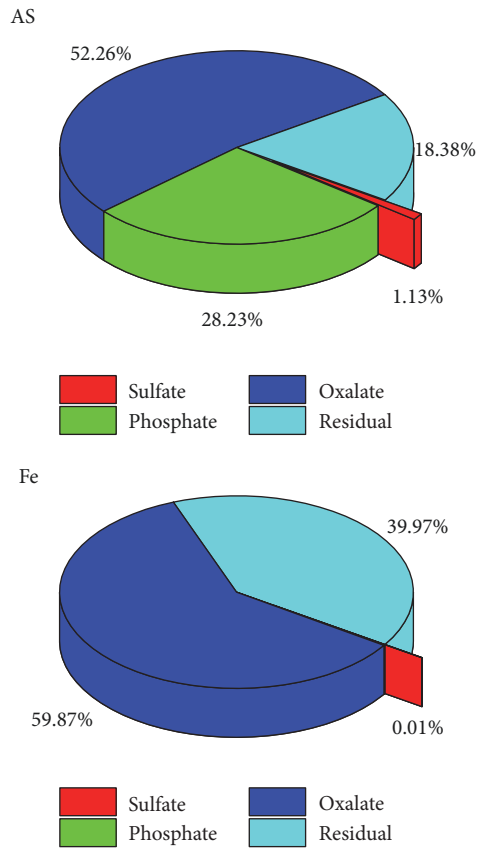

Figure 5: Distribution of As and Fe in the selective extractions.

results demonstrated that crystalline Fe oxides or carbonized phase is more efficient than amorphous iron oxyhydroxide in retaining arsenate in such irreversibly occluded forms. Only small amounts of As were present in the exchangeable fraction (1.13%), indicating that anion exchange from outer-sphere complexes was negligible. The regeneration of adsorbent is important in treating contaminated water for reducing the overall cost. The high proportion of As (70.64%) in the CS-Fe is associated with amorphous iron oxyhydroxide and in the residual, suggesting that CS-Fe does not have the advantage of regeneration ability. On the contrary, the less in the exchangeable and specifically adsorbed form, the better for the stabilization of As contaminated soil.

In summary, there are three mechanisms for arsenate sorption to the CS-Fe. First, a fraction of the arsenate is specifically adsorbed to the surface of both amorphous and crystalline Fe oxides. Second, substantial amounts of arsenate are strongly bound to amorphous iron oxyhydroxide via inner-sphere surface complexes. Third, partial occlusion of arsenate occurs on the crystalline Fe oxides or carbonized phase.

4. Conclusion

In the present study, iron-loaded biochar was successfully synthesized for arsenate removal. The maximum adsorption capacity estimated by the Langmuir model was 14.77 mg g^{-1}, which was comparable to and even moderately higher than many other iron-containing materials. The optimum pH range for arsenate removal was found to be between 2.0 and 8.0. Fe oxides including magnetite, natrojarosite, and amorphous iron oxyhydroxide constituted major As-adsorbing sinks. Further investigation into As speciation in the solid phase suggested that three mechanisms were involved in arsenate removal: sorption, strong inner-sphere surface complexes, and partial occlusion into the crystalline Fe oxides or carbonized phase. The biochar prepared from iron-impregnated corn straw may show better effects of remediation toward arsenic contaminated water or soil.

Conflicts of Interest

The authors declare that they have no conflicts of interest.

Acknowledgments

This project was financially supported by the National Natural Science Foundation of China (no. 41371320, no. 41371447, and no. 21677123).

Supplementary Materials

Table S1: sequential chemical extraction method for As-load biochar [21]. Figure S1: effect of CS-Fe dose on the adsorption of As(V) (experiment condition: the initial concentration of As(V) was 40 mg L^{-1}; the solid-to-liquid ratio was 5.0 g L^{-1} and stirred with 200 r min^{-1} at 30°C for 6 h). Figure S2: diagrams of As (V) species versus pH. *(Supplementary Materials)*

References

[1] X. Hu, Y. Zhang, J. Luo, M. Xie, T. Wang, and H. Lian, "Accumulation and quantitative estimates of airborne lead for a wild plant (Aster subulatus)," *Chemosphere*, vol. 82, no. 10, pp. 1351–1357, 2011.

[2] X. Bi, X. Feng, Y. Yang et al., "Allocation and source attribution of lead and cadmium in maize (Zea mays L.) impacted by smelting emissions," *Environmental Pollution*, vol. 157, pp. 834–839, 2009.

[3] T. Y. Lin, C. C. Wei, C. W. Huang, C. H. Chang, F. L. Hsu, and V. H. C. Liao, "Both phosphorus fertilizers and indigenous bacteria enhance arsenic release into groundwater in arsenic-contaminated aquifers," *Journal of Agricultural and Food Chemistry*, vol. 64, pp. 2214–2222, 2016.

[4] Z. Liu, F. S. Zhang, and R. Sasai, "Arsenate removal from water using Fe_3O_4-loaded activated carbon prepared from waste biomass," *Chemical Engineering Journal*, vol. 160, pp. 57–62, 2010.

[5] M. L. Sangyang, W. A. W. A. K. Ghani, A. Idris, and M. B. Ahmad, "Hydrogel biochar composite for arsenic removal from wastewater," *Desalination Water Treatment*, vol. 57, pp. 3674–3688, 2016.

[6] J. Zhu, Z. Lou, Y. Liu, R. Fu, S. A. Baig, and X. Xu, "Adsorption behavior and removal mechanism of arsenic on graphene modified by iron–manganese binary oxide (FeMnOx/RGO) from

aqueous solutions," *The Royal Society of Chemistry Advances*, vol. 5, pp. 67951–67961, 2015.

[7] N. Zhu, T. Yan, J. Qiao, and H. Cao, "Adsorption of arsenic, phosphorus and chromium by bismuth impregnated biochar: Adsorption mechanism and depleted adsorbent utilization," *Chemosphere*, vol. 164, pp. 32–40, 2016.

[8] T. Budinova, D. Savova, B.Tsyntsarski et al., "Biomass waste-derived activated carbon for the removal of arsenic and manganese ions from aqueous solutions," *Applied Surface Science*, vol. 255, no. 8, pp. 4650–4657, 2009.

[9] A. W. Samsuri, F. Sadegh-Zadeh, and B. J. Seh-Bardan, "Adsorption of As(III) and As(V) by Fe coated biochars and biochars produced from empty fruit bunch and rice husk," *Journal of Environmental Chemical Engineering (JECE)*, vol. 1, no. 4, pp. 981–988, 2013.

[10] E. Agrafioti, D. Kalderis, and E. Diamadopoulos, "Arsenic and chromium removal from water using biochars derived from rice husk, organic solid wastes and sewage sludge," *Journal of Environmental Management*, vol. 133, pp. 309–314, 2014.

[11] L. Z. Guan, J. J. Zhou, Y. Zhang, G. C. Zhang, J. H. Zhang, and Z. X. Chan, "Effects of biochars produced from different sources on arsenic adsorption and desorption in soil," *Chinese Journal of Applied Ecology*, vol. 24, no. 10, pp. 2941–2946, 2013.

[12] M. Jang, W. Chen, and F. S. Cannon, "Preloading hydrous ferric oxide into granular activated carbon for arsenic removal," *Environmental Science & Technology*, vol. 42, no. 9, pp. 3369–3374, 2008.

[13] S. Yao, Z. Liu, and Z. Shi, "Arsenic removal from aqueous solutions by adsorption onto iron oxide/activated carbon magnetic composite," *Journal of Environmental Health Science and Engineering*, vol. 12, no. 1, p. 58, 2014.

[14] J. Zhu, S. A. Baig, T. Sheng, Z. Lou, Z. Wang, and X. Xu, "Fe_3O_4 and MnO_2assembled on honeycomb briquette cinders (HBC) for arsenic removal from aqueous solutions," *Journal of Hazardous Materials*, vol. 286, pp. 220–228, 2015.

[15] Y. Jin, X. Liang, M. He, Y. Liu, G. Tian, and J. Shi, "Manure biochar influence upon soil properties, phosphorus distribution and phosphatase activities: A microcosm incubation study," *Chemosphere*, vol. 142, pp. 128–135, 2016.

[16] J. W. Gaskin, C. Steiner, K. Harris, K. C. Das, and B. Bibens, "Effect of low-temperature pyrolysis conditions on biochar for agricultural use," *Transactions of the Asabe*, vol. 51, no. 6, pp. 2061–2069, 2008.

[17] S. J. Lu, W. F. Tan, and L. Fan, "Point of zero charge (PZC) of manganese oxides determined with an improved salt titration method," *Acta Pedologica Sinica*, vol. 43, p. 763, 2006.

[18] D. Mohan, P. Singh, A. Sarswat, P. H. Steele, and C. U. Pittman, "Lead sorptive removal using magnetic and nonmagnetic fast pyrolysis energy cane biochars," *Journal of Colloid and Interface Science*, vol. 448, pp. 238–250, 2015.

[19] A. Contescu, C. Contescu, K. Putyera, and J. A. Schwarz, "Surface acidity of carbons characterized by their continuous pK distribution and Boehm titration," *Carbon*, vol. 35, no. 1, pp. 83–94, 1997.

[20] T. Sheng, S. A. Baig, Y. Hu, X. Xue, and X. Xu, "Development, characterization and evaluation of iron-coated honeycomb briquette cinders for the removal of As(V) from aqueous solutions," *Arabian Journal of Chemistry*, vol. 7, no. 1, pp. 27–36, 2014.

[21] B. Cances, F. Juillot, G. Morin et al., "XAS evidence of As (V) association with iron oxyhydroxides in a contaminated soil at a former arsenical pesticide processing plant," *Environmental Science & Technology*, vol. 39, pp. 9398–9405, 2005.

[22] D. Xu, Y. Zhao, K. Sun et al., "Cadmium adsorption on plant- and manure-derived biochar and biochar-amended sandy soils: impact of bulk and surface properties," *Chemosphere*, vol. 111, pp. 320–326, 2014.

[23] Y. Mikhaylova, G. Adam, L. Häussler, K. J. Eichhorn, and B. Voit, "Temperature-dependent FTIR spectroscopic and thermoanalytic studies of hydrogen bonding of hydroxyl (phenolic group) terminated hyperbranched aromatic polyesters," *Journal of Molecular Structure*, vol. 788, pp. 80–88, 2006.

[24] S. Y. Wang, Y. K. Tang, K. Li, Y. Y. Mo, H. F. Li, and Z. Q. Gu, "Combined performance of biochar sorption and magnetic separation processes for treatment of chromium-contained electroplating wastewater," *Bioresource Technology*, vol. 174, pp. 67–73, 2014.

[25] D. Bulgariu and L. Bulgariu, "Equilibrium and kinetics studies of heavy metal ions biosorption on green algae waste biomass," *Bioresource Technology*, vol. 103, no. 1, pp. 489–493, 2012.

[26] W. Chen, R. Parette, J. Zou, F. S. Cannon, and B. A. Dempsey, "Arsenic removal by iron-modified activated carbon," *Water Research*, vol. 41, no. 9, pp. 1851–1858, 2007.

[27] M. Li, Q. Liu, L. Guo et al., "Cu(II) removal from aqueous solution by Spartina alterniflora derived biochar," *Bioresource Technology*, vol. 141, pp. 83–88, 2013.

[28] S. Goldberg and C. T. Johnston, "Mechanisms of arsenic adsorption on amorphous oxides evaluated using macroscopic measurements, vibrational spectroscopy, and surface complexation modeling," *Journal of Colloid and Interface Science*, vol. 234, no. 1, pp. 204–216, 2001.

[29] A. Violante, S. D. Gaudio, M. Pigna, M. Ricciardella, and D. Banerjee, "Coprecipitation of arsenate with metal oxides. 2. Nature, mineralogy, and reactivity of iron (III) precipitates," *Environmental Science & Technology*, vol. 41, pp. 8275–8280, 2007.